BBA - Proteins and Proteomics 1866 (2018) 963–972

Contents lists available at ScienceDirect

BBA - Proteins and Proteomics

journal homepage: www.elsevier.com/locate/bbapap

Directed evolution and biophysical characterization of a full-length, soluble, human caveolin-1 variant

Joshua N. Smith[a], Joshua M. Edgar[b], J. Mark Balk[b], Mariam Iftikhar[b], Jessica C. Fong[c], Tivoli J. Olsen[b], Dmitry A. Fishman[b], Sudipta Majumdar[b], Gregory A. Weiss[a,b,*]

[a] Department of Molecular Biology and Biochemistry, University of California, Irvine, CA 92697, USA
[b] Department of Chemistry, University of California, Irvine, CA 92697, USA
[c] Department of Pharmaceutical Sciences, University of California, Irvine, CA 92697, USA

ARTICLE INFO

Keywords:
Phage display
Membrane proteins
Caveolin
Caveolae
Oligomerization
Biophysics

ABSTRACT

Protein engineering by directed evolution can alter proteins' structures, properties, and functions. However, membrane proteins, despite their importance to living organisms, remain relatively unexplored as targets for protein engineering and directed evolution. This gap in capabilities likely results from the tendency of membrane proteins to aggregate and fail to overexpress in bacteria cells. For example, the membrane protein caveolin-1 has been implicated in many cell signaling pathways and diseases, yet the full-length protein is too aggregation-prone for detailed mutagenesis, directed evolution, and biophysical characterization. Using a phage-displayed library of full-length caveolin-1 variants, directed evolution with alternating subtractive and functional selections isolated a full-length, soluble variant, termed cav_{sol}, for expression in *E. coli*. Cav_{sol} folds correctly and binds to its known protein ligands HIV gp41, the catalytic domain of cAMP-dependent protein kinase A, and the polymerase I and transcript release factor. As expected, cav_{sol} does not bind off-target proteins. Cellular studies show that cav_{sol} retains the parent protein's ability to localize at the cellular membrane. Unlike truncated versions of caveolin, cav_{sol} forms large, oligomeric complexes consisting of approximately > 50 monomeric units without requiring additional cellular components. Cav_{sol}'s secondary structure is a mixture of α-helices and β-strands. Isothermal titration calorimetry experiments reveal that cav_{sol} binds to gp41 and PKA with low micromolar binding affinity (K_D). In addition to the insights into caveolin structure and function, the approach applied here could be generalized to other membrane proteins.

1. Introduction

Approximately 30% of the human genome encodes membrane proteins (MPs). Essential roles fulfilled by MPs include ion transportation, energy generation, and signal transduction across the membrane [1]. Additionally, 60% of approved therapeutics target MPs, which illustrates the importance of MPs in medicine [2]. The hydrophobicity of transmembrane domains of MPs causes their aggregation upon removal from the membrane; this precipitation from solution complicates structural and biophysical characterization [1,3]. MPs thus represent only a fraction of the protein structures solved to date [4]. The field could benefit from new approaches to the solubilization and biophysical characterization of MPs interacting with their partners, as demonstrated here.

Caveolin-1 (cav) is a highly conserved 22 kDa monotopic MP with both N- and C- termini protruding into the cytoplasm [5,6]. Frequently found in endothelial cells and adipocytes, cav oligomerizes in vivo to force the cell membrane into 50–100 nm invaginations, termed caveolae [6,7]. At these caveolae-localized hubs, cav binds, inhibits and spatially localizes a number of cell signaling proteins [7,8,9]. Cav can also regulate cholesterol homeostasis by trafficking cholesterol to the cell membrane [6,10,11]. Cav can direct a clathrin-independent route to endocytosis through the caveolae. By this route, cav oligomers coat the caveolae, and cause its lipid membrane to pinch off during endocytosis [6,11]. Small molecules, soluble proteins and cell surface receptors can also enter the cell via caveolae. For example, caveolae endocytose the cholera toxin and the insulin-bound, activated insulin receptor [12,13].

Abbreviations: Cav, Caveolin-1; CD, Circular Dichroism; MALS, Multi-Angle Light Scattering; RALS, Right Angle Light Scattering; DoF, Degrees of Freedom; DLS, Dynamic Light Scattering; gp41, HIV glycoprotein 41; IMD, Intramembrane domain; ITC, Isothermal Titration Calorimetry; MBP, Maltose Binding Protein; MP, Membrane Protein; MW, Molecular Weight; PKA, the catalytic domain of cAMP-dependent protein kinase A; PTRF, Polymerase I and Transcript Release Factor; SEC, size exclusion chromatography; WT, wild-type

* Corresponding author at: Department of Chemistry, University of California, Irvine, CA 92697-2025, USA.
E-mail address: gweiss@uci.edu (G.A. Weiss).

https://doi.org/10.1016/j.bbapap.2018.05.014
Received 1 September 2017; Received in revised form 16 May 2018; Accepted 24 May 2018
Available online 29 May 2018
1570-9639/

In 2004, Yelick and co-workers demonstrated cav's importance to early development. Cav-knockout zebrafish embryos had phenotypic deficiencies within 12 h post knockout and failed to fully develop [14]. Phosphorylation of a specific cav residue (Y14) was shown to be a requirement for early development. Recent studies have demonstrated that cav knockout mice can survive, but have significantly reduced lifespans compared to control mice [15]. In summary, abundant evidence demonstrates the essential biological roles played by cav. Despite this importance, cav remains incompletely characterized biophysically and structurally due to its insolubility preventing recombinant overexpression of the full-length protein.

Cav is also implicated in a myriad of diseases including diabetes, heart disease, Alzheimer's disease, HIV infection, and cancer [7,11,16,17,18,19]. However, the mechanism through which cav contributes to these diseases often seems contradictory. For example, cav promotes tumor metastasis in certain cancers, and, in other tumor types, cav suppresses genes promoting cancer development and growth [20,21,22]. Furthermore, cav can be either over- or under-expressed in different tumor types [22,23,24]. Additionally, a dominant negative cav mutation, P132L, has been identified in breast cancer [25,26]. To resolve these issues, a need exists for tools to characterize cav binding and function.

The structure of cav dictates its multivariate and complex function. However, structural details of cav have remained elusive. To date, cav secondary structure analysis has applied truncated versions of the protein [27,28,29]. For example, the secondary structure of the caveolin scaffolding domain (CSD, residues 81–102) was mostly helical (63–75%) based on CD and NMR analysis of peptides representative of this domain (amino acid residues 81–101 and 81–109) [27,30]. The percentages of helical content varied between these two different constructs, suggesting that the length of the peptide could alter secondary structure. Analysis of a longer peptide (residues 81–132) revealed that the CSD includes β-strand character, while the IMD retains its helicity [28]. NMR analysis of a longer truncated cav construct (residues 62–178) suggests that the CSD is mostly helical, as are the IMD and C-terminal domains [29]. Thus, understanding of cav structure evolves with the increasing length of the construct analyzed, which motivated us to develop methods to examine full-length cav.

In addition to the length of the peptide examined, the environment surrounding the construct also plays a key role in its secondary structure. For example, the CSD appears α-helical when observed in the presence of dodecylphosphocholine (DPC) micelles, which are commonly used as a generic membrane mimetic [27]. In contrast, the CSD contains β-strand character in the presence of cholesterol rich lipid bilayers; the latter environment is designed to more closely resemble the native lipid composition of caveolae [28]. Thus, previous studies lacking a full-length construct showed that the secondary structure of cav is dependent on both the length of the examined construct and its environment.

As a scaffold or hub protein, cav organizes binding complexes with several different intracellular binding partners. For example, Polymerase I and Transcript Release Factor (PTRF or cavin) [31], endothelial Nitric Oxide Synthase (eNOS) [32], adenylyl cyclase [33], the catalytic subunit of cAMP-dependent protein kinase A (PKA) [30,34], and the HIV glycoprotein 41 (gp41) [35] bind, and are enzymatically inhibited by cav. PTRF has been shown to be required for caveolae formation through a direct interaction with cav at the cellular membrane [31,36]. Additionally, Nassoy and coworkers show that cells can respond to mechanical stress by quickly disassembling caveolae through disruption of the PTRF-cav interaction, providing extra stretchability for the lipid membrane [37]. Cav regulates eNOS, adenylyl cyclase, and PKA by inhibiting their catalysis [32,33,34]. Cav has been shown to inhibit HIV envelope-induced bystander apoptosis of SupT1 cells and $CD4^+$ T lymphocytes through its interaction with gp41 [38]. We have previously reported that cav binds very weakly to the anti-HIV drug T20 (trade name Fuzeon); ligands derived from the drug, however, bound with 7500-fold higher affinity [39,40]. T20 was derived from the gp41 region thought to bind to cav, and therefore could bind in a similar way.

A widely applied protein engineering technique, phage display genetically fuses a peptide or protein of interest to a coat protein of the M13 bacteriophage. First described by Smith and coworkers in 1985 [41], phage display was initially limited to display of peptides, but has since been extended to the display of several polypeptides, including antibodies [42,43], protein scaffolds [44,45,46], and hormones [47]. Upon successful display of the protein of interest on the phage surface, mutagenesis by either targeted or random substitutions can diversify the phage-encapsulated DNA. Growth in the presence of helper phage can then provide the resultant protein libraries [47]. Selections can isolate members of the library with a desired trait, such as thermal stability [48], solubility [36], binding affinity, or function [44,45].

Our laboratory has reported a new type of helper phage, termed M13-KO7$^+$, which allows the display of MPs, such as cav, on the surface of filamentous bacteriophage [49,50]. In previous experiments, selections with phage-displayed cav variants identified cav variants (e.g., gen-1a through gen-1e) capable of overexpression as fusion proteins in *E. coli*; as described above, wild-type (WT) cav fails to overexpress in *E. coli*. However, one cav variant from this first generation library (cav-11) could be overexpressed upon fusion to maltose binding protein (MBP). Subsequent attempts at biophysical and structural characterization were dominated by the large size of MBP (approx. Two times the MW of cav) [36]. Attempts to remove the MBP after proteolysis failed consistently. Here, we report a full-length, soluble and functional variant of cav, which does not require fusion to a solubilization domain. This variant allows biophysical characterization, including cav_{sol}'s secondary structure, oligomerization, and binding to its known binding partners.

2. Materials and methods

2.1. Library construction and phage-based selections

A phage-displayed library of caveolin-1 variants was constructed as previously described [36] with oligonucleotides encoding the substitutions shown in Table 1A. Four rounds of dual subtractive and functional selections were performed as previously described [36].

2.2. Subcloning for protein overexpression

The gp41 ectodomain (residues 546 to 578 and 624 to 655) and PTRF were subcloned for overexpression as previously described [36]. The gene for the catalytic domain of PKA (Addgene) was subcloned into a pET28c vector using the *Nco*I and *Bam*HI restriction sites. The caveolin variants isolated after four rounds of selections were amplified en masse by PCR using primers designed to introduce *Bam*HI and *Eco*RI restriction sites at the 5′ and 3′ termini respectively. This PCR amplicon was then subcloned into the pET28c vector using its BamHI and EcoRI restriction sites.

2.3. Protein overexpression and purification

Protein overexpression was performed in *E. coli* BL21 (DE3) cells. Cells containing DNA encoding either gp41, PKA, or PTRF were grown from seed cultures (10 mL seed/1 L culture) to an OD_{600} of 0.6 (37 °C). The cells were then induced for protein overexpression by addition of 0.5 mM IPTG, and incubated overnight with shaking at 22 °C (≈12 h). The cell pellets for gp41, PKA, or PTRF were collected, dissolved in lysis buffer (50 mM NaH_2PO_4 and 300 mM NaCl, pH 8.0, 10 mM 2-mercaptoethanol), and lysed via sonication. The crude cell lysates were incubated with IMAC resin (Ni^{2+}-NTA agarose) for 10–12 h at 4 °C. The resin-bound protein was washed with lysis buffer supplemented with 20, 30, or 40 mM imidazole (10 mL each). The protein was then eluted

Table 1
Designing a library of cav variants for directed evolution.*

	104			108				112				116				120				124				128				132
wild-type	S	A	L	F	G	I	P	M	A	L	I	W	G	I	Y	F	A	I	L	S	F	L	H	I	W	A	V	V	P
gen-1	-	-	R	D	-	-	-	-	-	V	N	R	-	-	D	V	-	-	-	-	V	Q	-	-	R	-	-	C	-
library	-	-	H	E	-	D	-	E	-	D	S	H	-	D	E	D	-	N	D	-	E	N	-	S	H	-	D	E	-
	-	-	R	D	-	I	-	M	-	V	N	R	-	I	D	F	-	H	L	-	D	H	-	N	R	-	H	D	-
	-	-	-	-	-	N	-	K	-	H	T	-	-	N	-	V	-	K	H	-	-	K	-	T	-	-	L	-	-
	-	-	-	-	-	V	-	V	-	L	V	-	-	V	-	Y	-	Q	V	-	-	Q	-	I	-	-	V	-	-

*Library substitutions shown in purple replaced key WT cav residues in the IMD to improve upon the first generation cav variant (gen-1, green). Hyphen indicates the wild-type amino acid.

with 250 mM imidazole (50 mL). The eluted gp41, PKA, or PTRF were then incubated with TEV protease to remove the His_6 tag and analyzed for purity by SDS-PAGE (15%).

Cells transformed with pET28c vector encoding cav_{sol} were incubated at 37 °C until reaching an OD_{600} of 0.8, and induced by addition of 0.5 mM IPTG for 3 h at 37 °C before collection. The cav_{sol} cell pellets were resuspended in lysis buffer A (50 mM Tris-HCl, 10 mM NaCl, 5 mM EDTA, pH 8.0), and lysed via sonication. The lysate was then centrifuged (30,996 × *g*, 45 min), and the resulting pellet was washed with wash buffer B (20 mM Na_2HPO_4, 20 mM NaCl, 5 mM EDTA, 25% w/v sucrose, pH 7.2) to further isolate the cav_{sol} present in the inclusion bodies. This solution was centrifuged again (30,996 x*g*, 45 min), and the resulting pellet was dissolved in denaturing buffer (8 M urea, 50 mM Tris HCl, 50 mM NaCl, pH 8.0) at 4 °C overnight with gentle shaking (≈150 rpm). The soluble, denatured protein was incubated with Ni^{2+}-charged IMAC resin for 10–12 h at 4 °C. This flow through was collected, and the resin-bound protein was washed with denaturing buffer at pH 8.0 and pH 5.5 (20 mL each), before elution in denaturing buffer at pH 4.0 (50 mL). The eluted protein was dialyzed for four days in refolding buffer (50 mM Tris-HCl, pH 8.0) to yield soluble, refolded protein. Protein purity was analyzed by 15% SDS-PAGE (Fig. S3). The protein was then concentrated and purified further using size exclusion chromatography (SEC) as described below.

2.4. ELISAs

ELISAs were used to assess protein-protein binding interactions as previously described [36]. Target proteins were coated on a 96-well microtiter plate at a concentration of 10 μg/mL. The plates were blocked with 0.2% nonfat milk (NFM), bovine serum albumin (BSA), ovalbumin, or casein, and the indicated concentrations of cav_{sol} in PBS supplemented with 0.2% nonfat milk and 0.05% Tween-20 were added. A mouse anti-His_6 epitope primary antibody (Sigma) and an anti-mouse horseradish peroxidase (HRP) conjugated secondary antibody (Sigma) were added to detect the presence of bound protein.

2.5. Circular dichroism

The circular dichroism spectrum of cav_{sol} was obtained using a Jasco J-810 Spectropolarimeter. Cav_{sol} was dialyzed into PBS and diluted to 4 μM for CD analysis at 20 °C. Six continuous wavelength scans from 195 to 255 nm were averaged with a data pitch of 1 nm, a 2.0 s response time, a 0.1 cm pathlength, and a 5 nm/min scanning speed (Fig. 3A). For the cav_{sol}-DPC CD experiment, a sample of 4 μM cav_{sol} was examined (Fig. S5). After this CD scan, 50 mM DPC was added to the same sample, which was again analyzed by CD. Conditions remained the same for this experiment with the exception of the number of scans, which was reduced to 2. A Sovitzky-Golay smoothing filter was applied to smooth the baseline. An online CD analysis program, Dichroweb [51], was used to estimate percentages of secondary structure.

2.6. Dynamic light scattering

The Dynamic Light Scattering spectrum of cav_{sol} was acquired on a Malvern Zetasizer Nano ZS instrument. Cav_{sol} was dialyzed into PBS and diluted from a concentration of ≈300 μM to 8 μM for DLS analysis. The spectrum was obtained from the backscatter, applying the general purpose analysis method with "protein" as the material and "water" as the dispersant at 20 °C.

2.7. SEC

The SEC spectrum of cav_{sol} was acquired using a Bio-Rad BioLogic DuoFlow Chromatography system equipped with a GE HiLoad 16/60 Superdex 200 PG gel filtration column. The gel filtration standard (Bio-Rad) was dissolved in 50 mM Tris-HCl pH 8.0, and used for column calibration. Cav_{sol} was refolded via dialysis into refolding buffer as described above, and was purified through the column described above.

2.8. SEC coupled to multi-angle static light scattering (SEC-MALS)

Protein samples at four concentrations, 120, 361, 724, and 923 μM were analyzed by static light scattering. Samples were auto-injected onto a aqueous gel permeation chromatography (GPC) column (A7000, column 300 × 8.0 mm, Viscotek, Malvern) at a flow rate of 1 mL/min in buffer (50 mM TrisHCl, pH 8.0) at a detector temperature of 20 °C and column temperature of 30 °C. The column is in-line with the following detectors: Viskotek 305 TDA MALS detector (Malvern) with a built-in refractometer (refractive index detector), and Zetasizer μV as a right angle light scattering (RALS) detector. The later, when attached to the GPC/SEC system generates absolute size and molecular weight of the samples. Masses were calculated with Malvern OmniSec software, with the dn/dc value set to 0.185 mL/g. BSA (ThermoFisher Scientific) was used as the calibration standard.

2.9. Isothermal titration calorimetry

ITC experiments were performed on a Malvern Microcal VP-ITC instrument. Nine injections of 5 μL followed by thirty-six injections of 7 μL of 300 μM cav_{sol} were added via a microsyringe in 400 s intervals to a solution of 62.5 μM gp41 with stirring at 307 rpm in 50 mM Tris-HCl, 5 mM 2-mercaptoethanol, pH 8.0 at 20 °C. Five injections of 5 μL followed by thirty-three injections of 7 μL of 300 μM cav_{sol} were added

via a microsyringe in 400 s intervals to a solution of 73.5 μM PKA with stirring at 307 rpm in 50 mM Tris-HCl, 5 mM 2-mercaptoethanol, pH 8.0 at 20 °C. The experimental data were obtained from fitting the titration curve using the Origin software provided with the instrument.

2.10. Cell culture and transfection

The genes for WT cav and cav_{sol} were cloned into a pBMN322 vector containing a mCherry tag (Addgene) flanked by *Eco*RI and *Bam*HI restriction sites. The constructs were independently cloned into HEK 293 cells (ATCC) using 500 ng of DNA and lipofectamine 2000 reagent (Invitrogen). HEK 293 cells were cultured in DMEM Media (Life Technologies) supplemented with antibiotics, sodium pyruvate, and 10% v/v fetal bovine serum. Cells were grown for 72 h post-transfection at 37 °C and 5% CO_2 before being supplemented with media containing geneticin (500 μg/mL, Life Technologies) to select for successfully transfected cells. Cells were selected with geneticin for two weeks before analysis by confocal microscopy.

2.11. Confocal microscopy

Transfected cells were grown on treated microscope slides (Thermo Fisher) for 3 days before fixation with 3.75% glutaraldehyde solution for 10 min. The cells were stained with CellMask Green (Thermo Fisher) for 10 min, and then with DAPI before being sealed with a coverslip and analyzed for the fluorescence. Fluorescent images were obtained using a Zeiss LSM 700 confocal microscope under a 60× objective with oil immersion. Images were analyzed using Velocity cell imaging software.

3. Results

3.1. Phage-displayed selection of a soluble human cav variant

Previously reported attempts to solubilize cav include isolation of cav-11 [36] (termed gen-1a here), which guided the design of a new library of cav variants, termed gen-2 (Table 1). Mutations targeted large, nonpolar, hydrophobic residues of the cav variant's intramembrane domain (IMD). Such residues were altered through changes to their DNA to include charged, polar, and, when accessible with a maximum of four substitutions per codon, the WT amino acid. Codons encoding aromatic residues, for example, were replaced with a mixture of codons designating aspartic acid, glutamic acid, arginine, or histidine substitutions. Due to the degeneracy of the genetic code, some additional amino acid substitutions were included. For example, the library was designed to substitute M111 with either a Lys, Glu, or Met residue. However, to encode these mutations, a Val substitution was also included in the library. The library's actual diversity (7.0×10 [8]), as measured by titers following electroporation to form the library, exceeded its theoretical diversity of 5.3×10 [8] variants.

Dual positive and negative selections isolated members of the library retaining both functionality and solubility, respectively (Fig. 1a). The negative or subtractive selections removed hydrophobic variants adhering to hydrophobic interaction chromatography resin (i.e., binding to butyl sepharose). The subsequent positive or functional selections collected library members capable of folding and binding to gp41. Each round of selections increased the stringency of both selection conditions. Increasing the ionic strength of the buffer, for example, strengthened the hydrophobic interactions during the subtractive selections for insolubility.

Increasing the number of washes during the functional selections identified more stable, better binding, and potentially better-folded cav variants (Fig. 1b). After four rounds of selections for functionality and solubility, genes encoding the selected variants were amplified by PCR and sub-cloned for protein overexpression in *E. coli* (Fig. S1). Several variants expressed to high levels in *E. coli* (Fig. S2). Sequence analysis of these variants identified the IMD substitutions responsible for increasing cav solubility (Table 2).

3.2. Expression, folding, and functional characterization of cav_{sol}

The cav variants identified through the selection process overexpress readily in *E. coli* inclusion bodies for subsequent protein folding. Unlike the gen-1 selectants, no fusion to MBP was required. The variant exhibiting the highest levels of protein overexpression (Fig. S2), termed cav_{sol}, was chosen for biophysical analysis (Table 2, gen 2d). After dissolving the inclusion bodies in urea and slowly removing the urea by multi-step dialysis, cav_{sol} remained in solution. Purification by FPLC using immobilized metal affinity chromatography and SEC (Fig. S3) yielded approximately 10 mg cav_{sol} per liter of culture with an estimated homogeneity of 95% by Image J analysis (Fig. S3) [52].

To compare cav_{sol}'s functionality with WT cav, we examined the variant's ability to interact with cav's known binding partners, including gp41, PKA, and PTRF. Cav_{sol} bound to all three binding partners in a dose-dependent manner by ELISA (Fig. 2A, B, and C). To investigate whether this binding was specific, cav_{sol}'s binding to a variety of additional, off-target proteins was examined. Cav_{sol} only binds to the known cav binding partners, and fails to bind any of the other off-target proteins tested (Fig. 2D). Taken together, the data strongly supports the hypothesis that cav_{sol} forms the correct folding conformation expected for WT caveolin.

3.3. Biophysical analysis of cav_{sol}

Two spectroscopic techniques measured cav_{sol}'s secondary structure and putative oligomeric states. Although cav_{sol} appears unstable in pure, deionized water, the protein remains stable in buffer (e.g., 20 mM Tris-HCl, pH 8.0) for many weeks at 4 °C. Circular Dichroism (CD) was used to verify the protein folding (Fig. 3A). Using Dichroweb, a tool for analyzing CD spectra [51], cav_{sol} was shown to include both α-helices and β-strands, The results are consistent with reported measurements with truncated cav variants [27,28,29]. Taken together, the CD and binding analysis suggest that cav_{sol} folds correctly.

Next we investigated perhaps the most defining characteristic of cav, its oligomerization to form caveolae [6,7,11]. To investigate cav_{sol}'s oligomeric state, we examined the particle size of cav_{sol} at multiple concentrations using dynamic light scattering (DLS). The DLS results show that cav_{sol} increases in particle size proportionally with an increase in concentration (Fig. 3B). Even at the lowest concentrations, cav_{sol} is approximately 35 nm in diameter, ranging to approximately 90 nm at the highest concentration tested. This size indicates that cav_{sol} forms large, concentration-dependent, oligomeric complexes.

To estimate the molecular weight of the cav_{sol} oligomers, the protein was characterized at different concentrations by SEC-MALS attached to a RALS detector. These detectors play an important role in gel permeation chromatography analysis because of their ability to directly measure molecular weight distribution [53,54,55]. During analysis, BSA, used as a calibration standard, had a molecular weight of 66.65 kDa, as expected. The highest concentration of cav_{sol}, 923 μM clogged the sample preparation filters, and was not analyzed. However, molecular weights were calculated for the other protein concentrations. The three concentrations, 120, 361, and 724 μM had average molecular weights of 350 kDa, 2000 kDa, and 3500 kDa respectively (Fig. 3C); the full widths of the peak at half maximum for these protein concentrations are 1.09, 1.44, and 1.56 min respectively. Therefore, with an increase in protein concentration, broader peak distributions are observed. Consistent with the DLS data, cav_{sol} forms higher order oligomers with increased protein concentrations. In summary, two independent measurements demonstrate cav_{sol} forms large oligomeric complexes with an estimated copy number of > 50 cav_{sol} units.

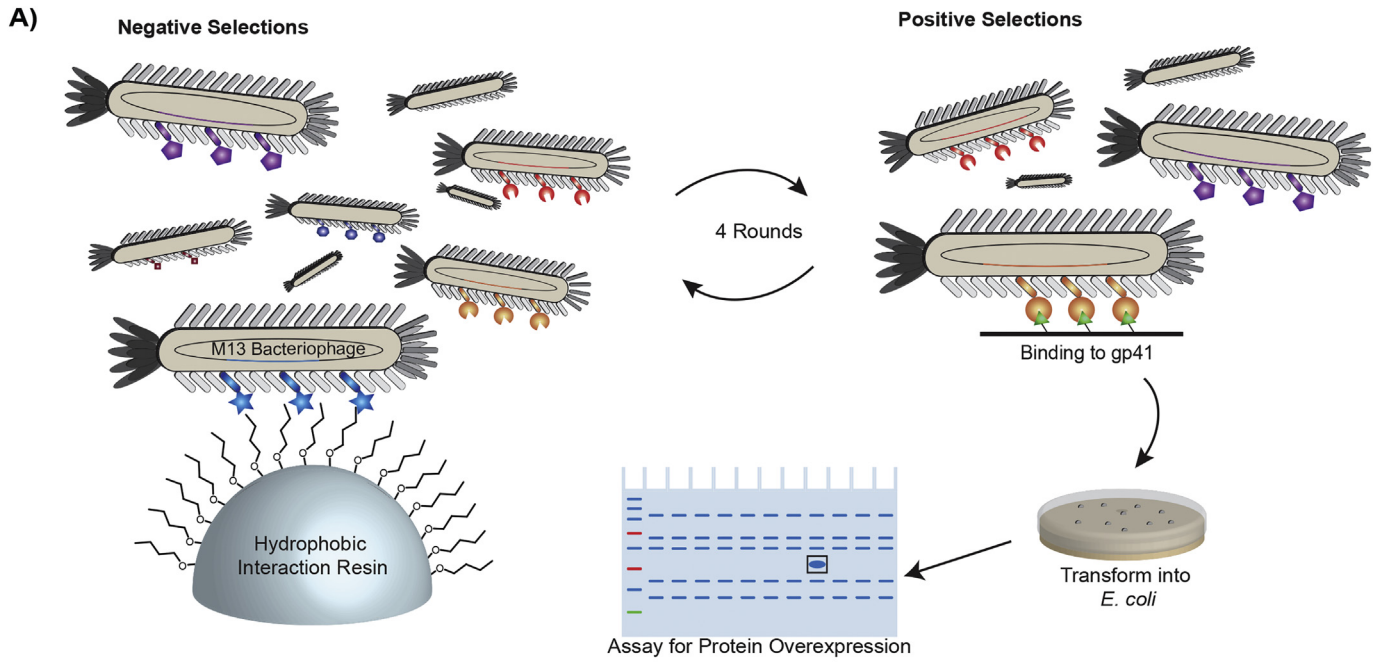

B)

Round	NaCl Conc. (M) (- selection)	# Washes (+ selection)	Blocking Agent (+ selection)	Titer
1	0.14	5	Casein	4.4×10^8
2	0.41	7	Nonfat Milk	7.9×10^5
3	1.20	9	BSA	3.0×10^4
4	3.70	11	Ovalbumin	8.1×10^5

Fig. 1. Selections for soluble and functional cav variants. (A) Schematic diagram detailing the selection and screening process. (i.) Negative selections removed hydrophobic, aggregation-prone variants. In the same round, (ii.) a positive selection tested binding to gp41. (iii.) After four rounds of selections, the DNA from remaining variants was transformed into *E. coli* and (iv.) screened for protein overexpression. This schematic diagram is not drawn to scale. (B) Conditions used for increasing stringency in each round of selection. Higher ionic strength buffer and additional washes increased the stringency of selection conditions for each round. To discourage nonspecific and off-target binding, the blocking agent was varied during rounds of selections.

3.4. Thermodynamic binding parameters between cav_{sol} and binding partners

Cav_{sol} allows direct observation of cav's interactions with its binding partners. ITC was used to determine thermodynamic parameters between cav_{sol}'s association with either gp41 or PKA. The titrations resulted in sigmoidal binding curves consistent with dose-dependent binding (Fig. 4). The fit for these curves follows a one-site binding model as determined through minimizing chi-squared for the fit to the curve (Fig. 4). Analysis of the ITC data reveals that cav_{sol} binds with modest affinity to both gp41 ($K_D = 0.844\,\mu M$) and PKA ($K_D = 0.670\,\mu M$). The stoichiometry of binding is three molecules of cav_{sol} per one gp41 or PKA molecule. Both binding events are exothermic and driven by enthalpic forces, rather than entropic considerations, as shown by the large, negative ΔH values (Fig. 4b).

3.5. The similar sub-cellular localization of both WT cav and cav_{sol} in cultured mammalian cells

To investigate whether or not cav_{sol} could still bind to the lipid membrane, we observed the localization pattern of the variant in human mammalian cells. Cav_{sol} and WT cav were fused with mCherry and transfected into HEK 293 cells. This cell line was chosen for its lack of caveolae resulting from low endogenous cav expression levels [56]. Confocal microscopy was then used to compare sub-cellular localization patterns of the two proteins (Fig. 5, Fig. S4). The contrast of the mCherry and CellMask Green plasmid marker images was increased to emphasize the appearance of the cavWT or cav_{sol} location and plasma membrane location respectively (Fig. 5). The image with original contrast is also shown (Fig. S4). This data suggests that cav_{sol} is still targeted to the membrane, and could function similarly to WT cav.

4. Discussion

Selections for cav solubility reveal preferred amino acid substitutions, and suggest strategies for the solubilization of other membrane proteins. The selections reported here identify caveolin variants capable of overexpression in *E. coli*; as noted earlier, WT cav cannot be overexpressed in bacterial cells. An important caveat is that these selections require binding to a target ligand, here gp41. Conceivably, the selected variant merely binds more tightly to gp41, than WT cav. However, experiments described below validate the hypothesis for selection on the basis of increased protein solubility, stability, and expression yields. Presumably, binding to gp41 and other binding partners remains

Table 2
Cav variants selected for solubility and function.

	104			108					112				116				120					124					128				132
wild-type	S	A	L	F	G	I	P	M	A	L	I	W	G	I	Y	F	A	I	L	S	F	L	H	I	W	A	V	V	P
*gen-1a	-	-	R	D	-	-	-	-	-	V	N	R	-	-	D	V	-	-	-	-	V	Q	-	-	R	-	-	C	-
gen-1b	-	-	R	D	-	-	-	-	-	-	-	-	-	-	D	D	-	N	R	-	Y	K	-	N	-	-	-	-	-
gen-1c	-	-	R	D	-	-	-	-	-	V	N	-	-	K	D	D	-	N	R	-	-	-	-	-	-	-	E	E	-
gen-1d	-	-	R	D	S	N	-	-	-	D	K	R	-	N	D	V	-	-	-	-	V	Q	-	-	R	-	-	-	-
gen-1e	-	-	-	D	-	-	-	-	-	V	N	R	-	K	D	V	-	-	R	-	-	M	-	N	R	T	D	-	-
gen-2a	-	-	R	D	-	N	-	V	-	-	T	R	-	V	E	D	-	N	V	-	E	H	-	-	H	-	-	E	-
gen-2b	-	-	R	E	-	N	-	E	-	-	S	H	-	-	E	-	-	K	V	-	D	K	-	S	R	-	-	D	-
gen-2c	-	-	R	D	-	-	-	V	-	-	T	R	-	V	E	D	-	N	V	-	E	H	-	-	H	-	-	E	-
†gen-2d	-	-	H	E	-	-	-	-	-	-	S	R	-	V	E	V	-	Q	V	-	D	H	-	-	R	-	D	D	-

*Renamed cav-11. †Renamed cav_{sol}.

unaffected, as residues in the CSD were not targeted by the library. The reported strategy should be applicable to any protein capable of display on the phage surface and separately a known, overexpressed binding target. As shown previously, MP phage display can include monotopic proteins like cav, but also transmembrane proteins, including ß-barrel MPs [49].

Comparing the sequences of several overexpressing cav variants isolated from the fourth round of gen-2 selections reveals important trends required for MP solubilization (Table 2). Overall, the vast majority of IMD substitutions found in these selectants encoded for polar amino acids, which validates the library design and solubilization strategy. However, several variants strongly selected nonpolar residues (e.g., valine) in specific IMD positions. For example, residues I117 and L122 were replaced with valine in the gen-2 selectants; far less preference for this non-polar residue was observed in the first generation of selections. The retention of nonpolar amino acids in these positions illustrates their importance to cav function and possibly structure in spite of strong selection for solubilizing amino acid sidechains. Thus, including the possibility for selecting WT residues appears critical to successful library-based MP solubilization.

Cav selectants for solubility from both gen-1 and gen-2 libraries strongly preferred charged amino acids at positions 106, 107, 115, 118, and 128 to replace hydrophobic sidechains. The addition of charged amino acids at these positions can increase protein solubility, while retaining cav function. Compared to gen-1a, cav_{sol} from gen-2 includes three additional charged amino acids at positions 124, 130, and 131. Glu and Asp were substituted interchangeably amongst the selected variants; therefore, the evolution conditions selected for sidechain charge, not structure. Aromatic amino acids at positions 107, 115, 118, and 128 were replaced with an Asp, Glu, Arg, or His residue in 89% of

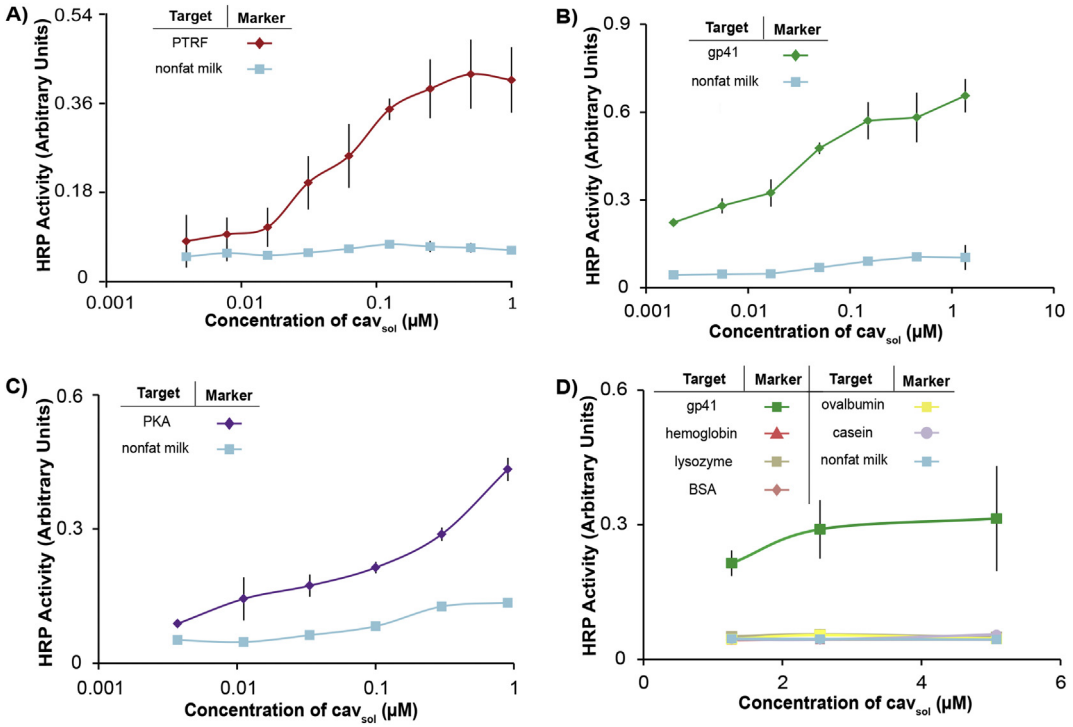

Fig. 2. Protein-based ELISAs investigating specific binding of cav_{sol} with its binding partners. Dose-dependent binding between cav_{sol} and (A) PTRF (red), (B) gp41 (green), or (C) PKA (purple) is observed. Cav_{sol} binds with moderate affinity and high specificity. (D) Notably, cav_{sol} does not bind nonspecifically to off-target proteins. All error bars report standard deviation from the mean (n = 3).

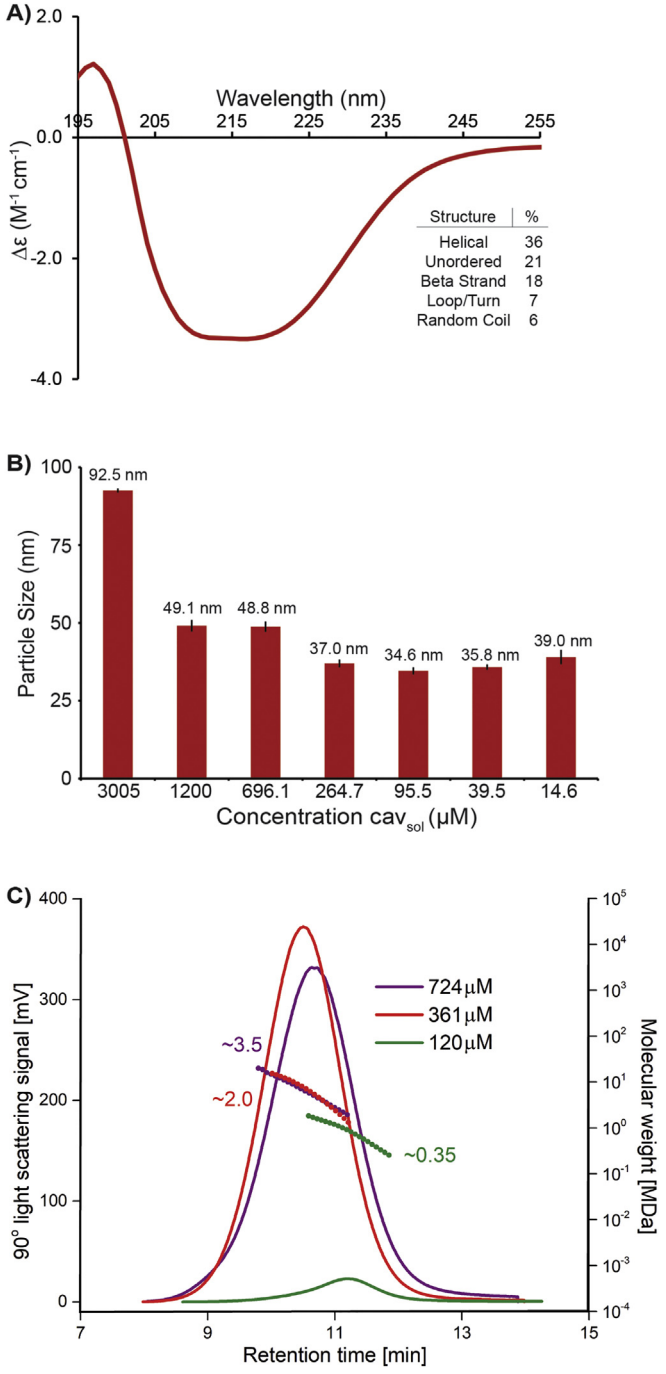

Fig. 3. Biophysical characterization of cav_{sol}. (A) CD spectrum of cav_{sol}. The CD spectrum of cav_{sol} reveals a highly helical secondary structure with some disordered regions and β-strands. The spectrum was obtained from averaging six continuous scans (B) Particle size of cav_{sol} at varying concentrations. Analysis by DLS shows a large particle size which increases proportionally with concentration. This suggests that cav_{sol} exists in an oligomeric form. Error bars denote standard deviation (n = 3). (C). SEC-MALS analysis of the cav_{sol} protein at three different concentrations. The SEC-MALS/ RI/ RALS were used to determine the cav_{sol} molecular masses using Malvern OmniSEC software. Chromatograms show the readings from the light scattering at 90° for the three different protein concentrations (120, 361, and 724 μM). The left and right axes represent the light scattering detector reading and molecular mass, respectively. The lines across the peaks indicate molar mass and homogeneity. Calculated molar masses are indicated.

the sequences selected. Interestingly, both Phe residues (positions 119 and 124) were replaced with a charged residue only 50% of the time. The remaining 50% retained the aromatic residue, or replaced it with a Val residue. The increased charge of gen-2 selectants could explain their greater solubility.

Cav functions as a protein scaffold, and mediates diverse cellular processes ranging from signal transduction to membrane trafficking [7]. Significantly, cav_{sol} retains the WT protein's ability to bind to gp41 and PKA as required for cav function. Furthermore, cav_{sol}'s binding to gp41 illustrates an unusual function of cav for preventing membrane hemifusion during viral assembly [38]. The direct cav-PTRF interaction remains little-explored, but is clearly supported through binding assays reported here with cav_{sol} and in other studies [31,36]. Caveolae spontaneously disassemble upon loss of PTRF. These results support a model where cav localizes several binding partners near the cell membrane and can interact directly with PTRF to form caveolae.

Cav_{sol}'s binding thermodynamics with gp41 and PKA were directly measured by ITC (Fig. 4). Both gp41 and PKA bind cav_{sol} with low micromolar K_D. Determining the stoichiometry of an interaction by ITC requires knowledge about the oligomerization state of the interacting species. For example, gp41 predominantly forms a dimer during bacterial overexpression (Fig. S5), and PKA remains monomeric. For both data sets, a single site binding model fit the ITC data best to minimize Chi [2]/DoF (Fig. 4B). The data also supports a model in which approximately three cav_{sol} molecules bind to each molecule of either dimeric gp41 or monomeric PKA. As shown by DLS and SEC-MALS (Fig. 3B, C), the oligomeric state of cav_{sol} increases with concentration. The concentration of cav_{sol} during ITC analysis was 300 μM. The observed molecular weight of cav_{sol} by SEC-MALS at a similar concentration (361 μM) was 2000 kDa equating to a complex consisting of ≈90 cav monomers. Thus, the ITC data suggests each oligomer of ≈90 cav_{sol} binds up to thirty ligands; the similar apparent affinities for gp41 and PKA measured here likely result in an equal molar distribution, assuming equal concentrations of each protein, of complexes with approximately fifteen of each protein binding to cav_{sol}.

Cav_{sol} uniquely allows analysis of the secondary structure for a full-length cav construct in the presence of different environments. The addition of dodecyl phosphatidylcholine micelles causes negligible difference in the CD spectra of cav_{sol} (Fig. S6). Thus, cav_{sol} retains its secondary structure in the presence this environment; the protein folds independently of the presence of a putative membrane mimic. This conclusion is further supported by cav_{sol}'s high solubility without requiring the addition of detergent. Additional CD analysis reveals a high percentage of α-helical secondary structure (36%) in cav_{sol} as shown by both the Dichroweb analysis and in characteristic depressions of the CD spectrum at approximately 215 and 207 nm [51] (Fig. 3A). This secondary structure analysis also suggests the presence of a moderate degree of β-strands (18%); similar results were obtained from analysis of a portion of the CSD by van der Wel and colleagues [28]. The disorder (21%) observed in the CD spectra of cav_{sol} suggests that some regions of the protein could be flexible and dynamic, a known property of its N-terminal domain [57]. In summary, this data provides the first direct measurement of the secondary structure of a full-length variant of cav, and finds support for a hybrid of the many models proposed for this protein.

Cav is widely recognized to form homoligomers inside the cell at the plasma membrane. Estimates of cav monomers per complex vary widely depending upon cell type, cellular location, and analytical technique used (Table S1). Early characterization of cav oligomers applied gradient centrifugation; the observed complexes consisted of 200, 400, or 600 kDa, which corresponds with approximately 9, 18, and 27 cav monomers respectively [58]. Furthermore, complexes comprised of cav monomers have been observed in mouse fibroblasts [59]. Cav_{sol} oligomerizes spontaneously upon refolding at modest concentrations (10–15 μM). As observed by DLS and SEC-MALS the protein rapidly forms higher order oligomers with increased protein concentrations. As

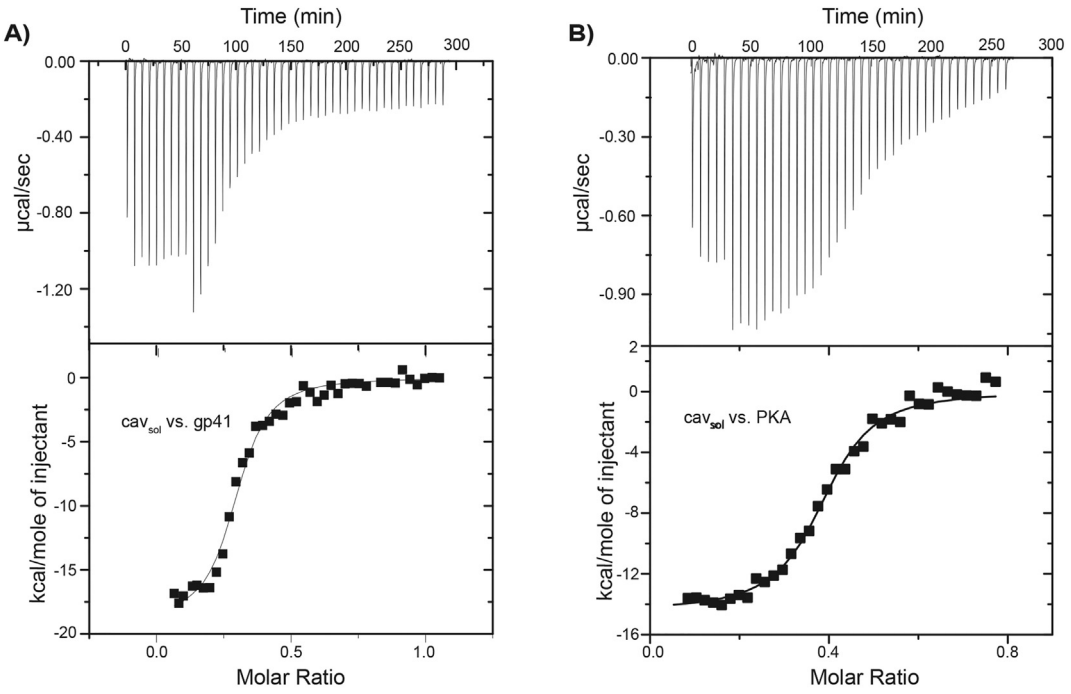

C)

Protein	Chi²/DoF x 10⁵	N	K_d (µM)	ΔG (kcal/mol)	ΔH (kcal/mol)	ΔS x 10⁻³ (kcal/mol/deg)
gp41	4.13	0.297 ± 0.005	0.844 ± 0.121	-7.97	-19.0 ± 0.458	-37.0
PKA	2.52	0.388 ± 0.004	0.670 ± 0.116	-8.20	-14.4 ± 0.233	-20.8

Fig. 4. Measuring binding between cav_{sol} and either (A) gp41 or (B) PKA by ITC. The upper panel depicts the calorimetric output from the cav_{sol} interaction with either gp41 (45 total injections of gp41) or PKA (38 total injections of PKA). The lower panel depicts integration of the calorimetric output, where the x-axis indicates the molar ratio of gp41 or PKA to cav_{sol}. The least squares fit is shown by the solid line. (C) ITC-derived thermodynamic binding parameters for interactions with cav_{sol}. Error indicates standard error.

observed by SEC-MALS, the MW ranged from 350 to 3500 kDa with increasing protein concentration. At the highest protein concentration analyzed by SEC-MALS, we estimate ≈160 cav monomers contribute to form the oligomeric complex, which provides the MW of 3.5 mDa (Fig. 3B, and C). These oligomers are very stable, and remain intact for weeks after formation despite 1000-fold dilution of the protein. Moreover, a broad range of oligomers form, as shown by the variation in particle size at increasing concentrations (Fig. 3B) and the heterogeneity of the observed MW within each concentration monitored by SEC-MALS (Fig. 3C). Interestingly, the particle size of the most concentrated oligomer measured by DLS (88 nm) is consistent with the approximate size observed for caveolae (50–100 nm) [6,7]. Furthermore, the DLS spectra suggest that cav_{sol} is not disproportionally long or wide in nature. For example, long rod-like proteins would show two distinct species by DLS: one species showing the diameter of the length of the rod, and another showing the width of the rod. Only one statistical distribution, although not homogenous as shown by the broadness of the peak, is observed in the DLS spectra of cav_{sol}, further supporting that cav_{sol} oligomers are largely symmetrical in nature.

We investigated cav_{sol} and WT cav localization in HEK 293 cells. The two proteins appear to localize to the same spots in the cell, predominantly the cellular membrane (Fig. 5, white arrows). Cav is known to have both N-terminal and C-terminal membrane binding domains that are required for internalization of the IMD. A construct containing only the IMD and not the membrane binding domains failed to internalize into the membrane [60]. The ability of cav_{sol} to localize at the cellular membrane despite substitutions to the IMD supports this observation, since the membrane binding domains were undisturbed. Both, WT cav and cav_{sol} appear not only to localize in the membrane, but also to form protein clusters at the membrane. Unfortunately, limits to the resolution of confocal microscopy prevent us from identifying these clusters as caveolae. In summary, the microscopy presented here demonstrates that substitutions to the cav IMD did not affect cav_{sol}'s ability to localize to the cell membrane.

In conclusion, we report the selection of the first known full-length cav variant able to overexpress to high levels in *E. coli* and remain soluble in vitro upon refolding. The variant, cav_{sol}, was shown by ELISA and ITC to interact with known binding partners, gp41, PKA, and PTRF, and exhibits the expected secondary structural characteristics evident in its CD spectrum. Cav_{sol} oligomerizes in a concentration-dependent manner into large complexes of 24 monomers approximately 88 nm in diameter as observed by SEC and DLS respectively at high concentrations. Despite substitutions to the IMD, cav_{sol} retains the localization associated with WT cav, including the cellular membrane. We have reported a small peptide capable of binding to cav_{sol} and disrupting its oligomerization [40]; this demonstrates that cav_{sol} provides a potential therapeutic target for drug development. Overall, cav_{sol} provides a powerful new tool for investigating the properties of cav structure and function.

Support

This work was supported by the NIH, specifically the National Institute of General Medical Sciences (Grants RO1GM078528-01 and 1RO1GM100700-01) and the National Institute of Allergy and Infectious Disease (training grant T32 AI007319).

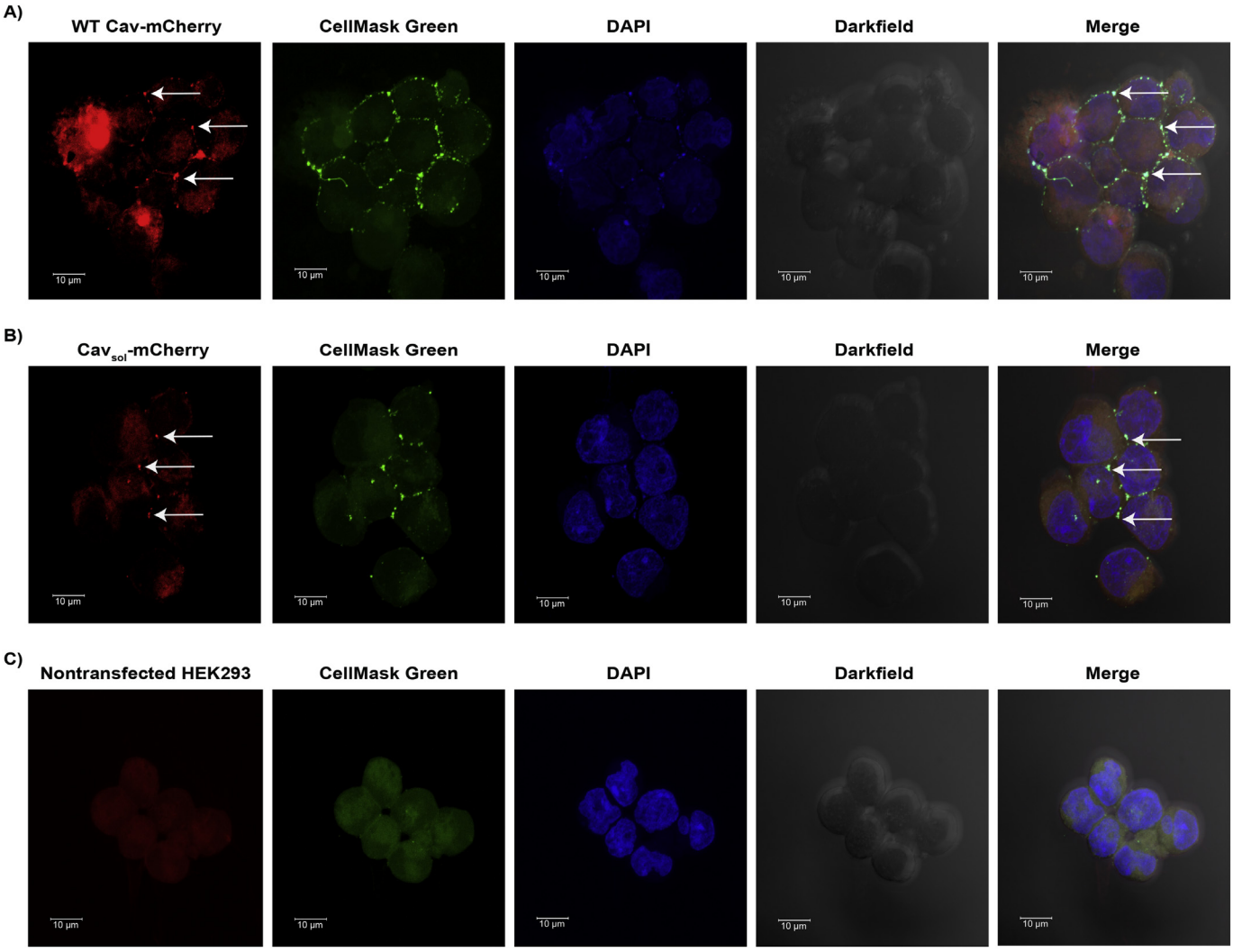

Fig. 5. Localization of WT cav or cav$_{sol}$ fused to mCherry in HEK 293 cells. HEK 293 cells transfected with either (A) WT cav-mCherry, (B) cav$_{sol}$-mCherry, or (C) non-transfected cells were observed using confocal microscopy. Cells were tested for mCherry fluorescence to identify the mCherry-fused cav, cellmask green fluorescence to identify the cell membrane, DAPI to identify DNA (cell nucleus), or with the darkfield setting to identify the cell outline. White arrows represent either WT cav or cav$_{sol}$ fluorescence. The contrast of select samples was adjusted to improve the image quality of select panels. The contrast of the WT Cav and Cav$_{sol}$-mCherry samples was increased by approximately 40%. The contrast of the WT Cav and Cav$_{sol}$ CellMask Green samples was increased by approximately 20%.

Acknowledgements

We thank Dr. Mark Richardson and Dr. Amanda Gilliam for helpful conversations, Kyle Roskamp for help with the SEC-MALS experiment, and Dr. Adeela Sayed for her help with microscopy. We also thank the Malvern Instruments analytical support team for help analyzing the ITC data.

Appendix A. Supplementary data

Supplementary data to this article can be found online at https://doi.org/10.1016/j.bbapap.2018.05.014.

References

[1] A. Engel, H.E. Gaub, Structure and mechanics of membrane proteins, Annu. Rev. Biochem. 77 (2008) 127–148.
[2] M.A. Yildirim, K.-I. Goh, M.E. Cusick, A.-L. Barabasi, M. Vidal, Drug-target network, Nat. Biotechnol. 25 (2007) 1119–1126.
[3] Y. He, K. Wang, N. Yan, The recombinant expression systems for structure determination of eukaryotic membrane proteins, Protein Cell 5 (2014) 658–672.
[4] E.P. Carpenter, K. Beis, A.D. Cameron, S. Iwata, Overcoming the challenges of membrane protein crystallography, Curr. Opin. Struct. Biol. 18 (2008) 581–586.
[5] J.R. Glenney, The sequence of human caveolin reveals identity with VIP21, a component of transport vesicles, FEBS Lett. 314 (1992) 45–48.
[6] T.M. Williams, M.P. Lisanti, The Caveolin Proteins, Genome Biol. 5 (2004) 214.1–214.8.
[7] T.M. Williams, M.P. Lisanti, The Caveolin genes: from cell biology to medicine, Ann. Med. 36 (2004) 584–595.
[8] M. Sargiacomo, P.E. Scherer, Z. Tang, E. Kubler, K.S. Song, M.C. Sanders, M.P. Lisanti, Oligomeric structure of caveolin: implications for caveolae membrane organization, Proc. Natl. Acad. Sci. U. S. A. 92 (1995) 9407–9411.
[9] K.T. Root, S.M. Plucinsky, K.J. Glover, Recent progress in the topology, structure, and oligomerization of caveolin: a building block of caveolae, Curr. Top. Membr. 75 (2015) 305–336.
[10] P.G. Frank, M.W.-C. Cheung, S. Pavlides, G. Llaverias, D.S. Park, M.P. Lisanti, Caveolin-1 and regulation of cellular cholesterol homeostasis, Am. J. Physiol. Heart Circ. Physiol. 291 (2006) H677–H686.
[11] A.W. Cohen, R. Hnasko, W. Schubert, M.P. Lisanti, Role of caveolae and caveolins in health and disease, Physiol. Rev. 84 (2004) 1341–1379.
[12] P.A. Orlandi, P.H. Fishman, Filipin-dependent inhibition of cholera toxin: evidence for toxin internalization and activation through caveolae-like domains, J. Cell Biol. 141 (1998) 905–915.
[13] S. Fagerholm, U. Örtegren, M. Karlsson, I. Ruishalme, P. Strålfors, Rapid insulin-dependent endocytosis of the insulin receptor by caveolae in primary adipocytes, PLoS One 4 (2009) e5985.1–e5985.10.
[14] P.K. Fang, K.R. Solomon, L. Zhuang, M. Qi, M. McKee, M.R. Freeman, P.C. Yelick, Caveolin-1α and -1ß perform nonredundant roles in early vertebrate development, Am. J. Pathol. 169 (2006) 2209–2222.
[15] D.S. Park, A.W. Cohen, P.G. Frank, B. Razani, H. Lee, T.M. Williams, M. Chandra, J. Shirani, A.P. De Souza, B. Tang, L.A. Jelicks, S.M. Factor, L.M. Weiss,

H.B. Tanowitz, M.P. Lisanti, Caveolin-1 null (-/-) mice show dramatic reductions in life span, Biochemistry 42 (2003) 15124–15131.
[16] A.W. Cohen, T.P. Combs, P.E. Scherer, M.P. Lisanti, Role of caveolin and caveolae in insulin signaling and diabetes, Am. J. Physiol. Endocrinol. Metab. 285 (2003) E1151–E1160.
[17] S.B. Gaudreault, D. Dea, J. Poirier, Increased caveolin-1 expression in Alzheimer's disease brain, Neurobiol. Aging 25 (2004) 753–759.
[18] S. Lin, P.E. Nadeau, X. Wang, A. Mergia, Caveolin-1 reduces HIV-1 infectivity by restoration of HIV Nef mediated impairment of cholesterol efflux by apoA-I, Retrovirology 9 (2012) 85.
[19] X.M. Wang, P.E. Nadeau, S. Lin, J.R. Abbott, A. Mergia, Caveolin 1 inhibits HIV replication by transcriptional repression mediated through NF-κB, J. Virol. 85 (2011) 5483–5493.
[20] U.E. Martinez-Outschoorn, F. Sotgia, M.P. Lisanti, Caveolae and signalling in cancer, Nat. Rev. Cancer 15 (2015) 225–237.
[21] L. Lobos-Gonzalez, L. Aguilar, J. Diaz, N. Diaz, H. Urra, V.A. Torres, V. Silva, C. Fitzpatrick, A. Lladser, K.S. Hoek, L. Leyton, A.F. Quest, E-cadherin determines Caveolin-1 tumor suppression or metastasis enhancing function in melanoma cells, Pigment Cell Melanoma Res. 26 (2013) 555–570.
[22] A.F. Quest, J.L. Gutierrez-Pajares, V.A. Torres, Caveolin-1: an ambiguous partner in cell signalling and cancer, J. Cell. Mol. Med. 12 (2008) 1130–1150.
[23] E.Y. Tse, F.C. Ko, E.K. Tung, L.K. Chan, T.K. Lee, E.S. Ngan, K. Man, A.S. Wong, I.O. Ng, J.W. Yam, Caveolin-1 overexpression is associated with hepatocellular carcinoma tumourigenesis and metastasis, J. Pathol. 226 (2012) 645–653.
[24] K. Wiechen, C. Sers, A. Agoulnik, K. Arlt, M. Dietel, P.M. Schlag, U. Schneider, Down-regulation of caveolin-1, a candidate tumor suppressor gene, in sarcomas, Am. J. Pathol. 158 (2001) 833–839.
[25] K. Hayashi, S. Matsuda, K. Machida, T. Yamamoto, Y. Fukuda, Y. Nimura, T. Hayakawa, M. Hamaguchi, Invasion activating caveolin-1 mutation in human scirrhous breast cancers, Cancer Res. 61 (2001) 2361–2364.
[26] H. Lee, D.S. Park, B. Razani, R.G. Russell, R.G. Pestell, M.P. Lisanti, Caveolin-1 mutations (P132L and null) and the pathogenesis of breast cancer: caveolin-1 (P132L) behaves in a dominant-negative manner and caveolin-1 (−/−) null mice show mammary epithelial cell hyperplasia, Am. J. Pathol. 161 (2002) 1357–1369.
[27] C. Le Lan, J.M. Neumann, N. Jamin, Role of the membrane interface on the conformation of the caveolin scaffolding domain: a CD and NMR study, FEBS Lett. 580 (2006) 5301–5305.
[28] C.L. Hoop, V.N. Sivanandam, R. Kodali, M.N. Srnec, P.C. van der Wel, Structural characterization of the caveolin scaffolding domain in association with cholesterol-rich membranes, Biochemistry 51 (2012) 90–99.
[29] S.M. Plucinsky, K.J. Glover, Secondary structure analysis of a functional construct of Caveolin-1 reveals a long C-terminal helix, Biophys. J. 109 (2015) 1686–1688.
[30] A.M. Levin, J.G. Coroneus, M.J. Cocco, G.A. Weiss, Exploring the interaction between the protein kinase A catalytic subunit and caveolin-1 scaffolding domain with shotgun scanning, oligomer complementation, NMR, and docking, Protein Sci. 15 (2006) 478–486.
[31] M.M. Hill, M. Bastiani, R. Luetterforst, M. Kirkham, A. Kirkham, S.J. Nixon, P. Walser, D. Abankwa, V.M.J. Oorschot, S. Martin, J.F. Hancock, R.G. Parton, PTRF-cavin, a conserved cytoplasmic protein required for caveola formation and function, Cell 132 (2008) 113–124.
[32] H. Ju, R. Zou, V.J. Venema, R.C. Venema, Direct interaction of endothelial nitric-oxide synthase and caveolin-1 inhibits synthase activity, J. Biol. Chem. 272 (1997) 18522–18525.
[33] Y. Toya, C. Schwencke, J. Couet, M.P. Lisanti, Y. Ishikawa, Inhibition of adenylyl cyclase by caveolin peptides, Endocrinology 139 (1998) 2025–2031.
[34] B. Razani, C.S. Rubin, M.P. Lisanti, Regulation of cAMP-mediated signal transduction via interaction of caveolins with the catalytic subunit of protein kinase a, J. Biol. Chem. 274 (1999) 26353–26360.
[35] A.G. Hovanessian, J.-P. Briand, E.A. Said, J. Svab, S. Ferris, H. Dali, S. Muller, C. Desgranges, B. Krust, The Caveolin-1 binding domain of HIV-1 glycoprotein gp41 is an efficient B cell epitope vaccine candidate against virus infection, Immunity 21 (2004) 617–627.
[36] A. Hajduczki, S. Majumdar, M. Fricke, I.A.M. Brown, G.A. Weiss, Solubilization of a membrane protein by combinatorial supercharging, ACS Chem. Biol. 6 (2011) 301–307.
[37] B. Sinha, D. Koster, R. Ruez, P. Gonnord, M. Bastiani, D. Abankwa, R.V. Stan, G. Butler-Browne, B. Vedie, L. Johannes, N. Morone, R.G. Parton, G. Raposo, P. Sens, C. Lamaze, P. Nassoy, Cells respond to mechanical stress by rapid disassembly of caveolae, Cell 144 (2011) 402–413.
[38] X.M. Wang, P.E. Nadeau, Y.T. Lo, A. Mergia, Caveolin-1 modulates HIV-1 envelope-induced bystander apoptosis through gp41, J. Virol. 84 (2010) 6515–6526.
[39] S. Majumdar, A. Hajduczki, R. Vithayathil, T.J. Olsen, R.M. Spitler, A.S. Mendez, T.D. Thompson, G.A. Weiss, In vitro evolution of ligands to the membrane protein caveolin, J. Am. Chem. Soc. 133 (2011) 9855–9862.
[40] A.J. Gilliam, J.N. Smith, D. Flather, K.M. Johnston, A.M. Gansmiller, D.A. Fishman, J.M. Edgar, M. Balk, S. Majumdar, G.A. Weiss, Affinity-guided design of caveolin-1 ligands for deoligomerization, J. Med. Chem. 59 (2016) 4019–4025.
[41] G. Smith, Filamentous fusion phage: novel expression vectors that display cloned antigens on the virion surface, Science 228 (1985) 1315–1317.
[42] J. Bazan, I. Całkosiński, A. Gamian, Phage display—a powerful technique for immunotherapy: 1. Introduction and potential of therapeutic applications, Hum. Vaccin. Immunother. 8 (2012) 1817–1828.
[43] J. McCafferty, A.D. Griffiths, G. Winter, D.J. Chiswell, Phage antibodies: filamentous phage displaying antibody variable domains, Nature 348 (1990) 552–554.
[44] R.J. Hosse, A. Rothe, B.E. Power, A new generation of protein display scaffolds for molecular recognition, Protein Sci. 15 (2006) 14–27.
[45] N. Zhao, M.A. Schmitt, J.D. Fisk, Phage display selection of tight specific binding variants from a hyperthermostable Sso7d scaffold protein library, FEBS J. 283 (2016) 1351–1367.
[46] E. Campbell, M. Kaltenbach, G.J. Correy, P.D. Carr, B.T. Porebski, E.K. Livingstone, L. Afriat-Jurnou, A.M. Buckle, M. Weik, F. Hollfelder, N. Tokuriki, C.J. Jackson, The role of protein dynamics in the evolution of new enzyme function, Nat. Chem. Biol. 12 (2016) 944–950.
[47] S. Bass, R. Greene, J.A. Wells, Hormone phage: an enrichment method for variant proteins with altered binding properties, Proteins 8 (1990) 309–314.
[48] K. Pershad, B.K. Kay, Generating thermal stable variants of protein domains through phage display, Methods 60 (2013) 38–45.
[49] R. Vithayathil, R.M. Hooy, M.J. Cocco, G.A. Weiss, The scope of phage display for membrane proteins, J. Mol. Biol. 414 (2011) 499–510.
[50] S. Majumdar, A. Hajduczki, A.S. Mendez, G.A. Weiss, Phage display of functional, full-length human and viral membrane proteins, Bioorg. Med. Chem. Lett. 18 (2008) 5937–5940.
[51] L. Whitmore, B.A. Wallace, DICHROWEB, an online server for protein secondary structure analyses from circular dichroism spectroscopic data, Nucleic Acids Res. 32 (2004) W668–W673.
[52] K.S. Song, Z. Tang, S. Li, M.P. Lisanti, Mutational analysis of the properties of caveolin-1. A novel role for the C-terminal domain in mediating homo-typic caveolin-caveolin interactions, J. Biol. Chem. 272 (1997) 4398–4403.
[53] P.J. Wyatt, Light-scattering and the absolute characterization of macromolecules, Anal. Chim. Acta 272 (1993) 1–40.
[54] J. Wen, T. Arakawa, J.S. Philo, Size-exclusion chromatography with on-line light-scattering, absorbance, and refractive index detectors for studying proteins and their interactions, Anal. Biochem. 240 (1996) 155–166.
[55] E. Folta-Stogniew, K.R. Williams, Determination of molecular masses of proteins in solution: implementation of an HPLC size exclusion chromatography and laser light scattering service in a core laboratory, J. Biomol. Tech. 10 (1999) 51–63.
[56] L. Wang, M.A. Connelly, A.G. Ostermeyer, H.-h. Chen, D.L. Williams, D.A. Brown, Caveolin-1 does not affect SR-BI-mediated cholesterol efflux or selective uptake of cholesteryl ester in two cell lines, J. Lipid Res. 44 (2003) 807–815.
[57] J. Kim, J. Shin, H. Park, Structural characterization for N-terminal domain of caveolin-1, Korean J. Biol. Sci. 7 (2003) 207–211.
[58] S. Monier, D.J. Dietzen, W.R. Hastings, D.M. Lublin, T.V. Kurzchalia, Oligomerization of VIP21-caveolin in vitro is stabilized by long chain fatty acylation or cholesterol, FEBS Lett. 388 (1996) 143–149.
[59] L. Pelkmans, M. Zerial, Kinase-regulated quantal assemblies and kiss-and-run recycling of caveolae, Nature 436 (2005) 128–133.
[60] A. Schlegel, M.P. Lisanti, A molecular dissection of caveolin-1 membrane attachment and oligomerization. Two separate regions of the caveolin-1 C-terminal domain mediate membrane binding and oligomer/oligomer interactions in vivo, J. Biol. Chem. 275 (2000) 21605–21617.